Received: 26 June 2020 | Revised: 13 November 2020 | Accepted: 20 November 2020

DOI: 10.1002/jms.4692

RESEARCH ARTICLE

Journal of MASS SPECTROMETRY WILEY

Characterization of defined sulfated heparin-like oligosaccharides by electrospray ionization ion trap mass spectrometry

Katharina Lemmnitzer[1] | Sebastian Köhling[2] | Joanna Freyse[2] | Jörg Rademann[2] | Jürgen Schiller[1]

[1]Faculty of Medicine, Institute of Medical Physics and Biophysics, University of Leipzig, Leipzig, Germany

[2]Department of Biology, Chemistry, and Pharmacy, Institute of Pharmacy, Pharmaceutical and Medicinal Chemistry, Free University of Berlin, Berlin, Germany

Correspondence
Katharina Lemmnitzer, Faculty of Medicine, Institute of Medical Physics and Biophysics, University of Leipzig, Härtelstraße 16-18, D-04107 Leipzig, Germany.
Email: katharina.lemmnitzer@medizin.uni-leipzig.de

Funding information
Deutsche Forschungsgemeinschaft, Grant/Award Number: 59397982-TRR67(A8)

Abstract

Glycosaminoglycans (GAG) as long, unbranched polysaccharides are major components of the extracellular matrix. Many studies provided additional evidence of a specific binding between mediators and sulfated GAG, at which the sulfation code—which means the number and positions of sulfate groups along the polysaccharide chain—plays an important role.

GAG from natural sources are very inhomogeneous regarding their sulfation patterns and molecular weight. Additionally, there is a high risk of contamination. This results in a growing interest in the careful characterization of native GAG and the synthesis of artificial GAG. Additionally, chemically oversulfated GAG analogues show many favorable properties. However, the structural characterization of these carbohydrates by mass spectrometry remains challenging. One significant problem is the sulfate loss during the ionization, which increases with the number of sulfate residues.

We used the sulfated pentasaccharide fondaparinux as model substance to optimize sample preparation and measurement conditions, compared different established desalination methods and already existing protocols for sulfated oligosaccharides, and investigated their impact on the quality of the mass spectra. After optimization of the measurement conditions, we could establish a gentle and fast protocol for the mass spectrometry characterization of (fully) sulfated, artificial GAG-like oligosaccharides with minimized sulfate loss in the positive and negative ion mode. Here, the negative ion mode was more sensitive in comparison with the positive one, and fondaparinux species with sulfate loss were not detectable under the optimized conditions in the positive ion mode.

KEYWORDS

(over)sulfation, desalination, ESI (IT) MS, fondaparinux, glycosaminoglycans, sulfate loss

1 | INTRODUCTION

Glycosaminoglycans (GAG) as important building blocks of proteoglycans are major constituents of the extracellular matrix (ECM).[1] GAG vary not only in the length and the monosaccharide composition but also in the type of the glycosidic linkages and the number and positions of sulfate residues along the chains.[2] Hyaluronan (HA) is the only non-sulfated GAG and consists of repeating disaccharide units of D-*N*-acetylglucosamine (GlcNAc) and D-glucuronic acid (GlcA) linked by alternating β-1 → 3 and β-1 → 4 glycosidic linkages.[3] All other GAG are modified by post-translational modifications: in particular, *O*-sulfation (sulfuric acid mono-ester) occurs resulting in polysaccharides such as chondroitin sulfate (CS).[4] N-sulfation, which is typical of heparin, may also occur.[5]

These long, unbranched, often sulfated polysaccharides do not only define the structure and biophysical properties of the respective tissue but also affect the embedded cells via their surface receptors and the interaction with different signaling molecules such as interleukins and growth factors. Therefore, GAG possess a considerable influence on tissue development and morphogenesis.[6–8] The interest in GAG is not only based on the medical aspects of the native ECM[9,10] and potential curative pathways: GAG additionally represent components of artificial ECM for cartilage and bone regeneration[11] as well as targets for different pharmacological applications.[12–15]

Thereby, the function of GAG in the ECM is considered as mainly structure-bearing by the significant water-binding capacity of GAG.[16,17] However, a variety of studies provided evidence of a specific binding between mediators and sulfated GAG, at which the sulfation code—which means the number and positions of sulfate groups along the polysaccharide chain—plays an important role.[18]

GAG are highly diverse because the sulfation pattern is the result of post-translational modifications of the polysaccharide chain by different sulfotransferases. Thus, GAG from native sources, such as bovine or shark tissues, are rather inhomogeneous regarding not only their monosaccharide composition and the chain length but also the position and number of sulfate residues.[19]

The interest in (sulfated) GAG has considerably increased during the last years. Besides their use in the treatment of musculoskeletal diseases (such as arthrosis),[20] selected GAG (such as heparin) are also used as drugs—particularly due to their function as anticoagulants.[21] These effects are significantly depending on the sulfation pattern of the applied GAG: the heparin contamination crisis[22] has tremendously emphasized this aspect and pointed out that the chemical, as well as biochemical characterization of GAG, is extremely important.[23]

Additionally, there are increasing indications that oversulfated GAG are very promising molecules.[24] For instance, there is evidence that the coating of (metallic) implants with chemically oversulfated HA improves the incorporation of the implant into the tissue: it is also argued that these strongly acidic compounds specifically attract tissue cells and favor in this way tissue regeneration, which additionally improves the stability of the implant within the tissue.[25]

Oligosaccharides from natural GAG with a moderate extent of sulfation can be routinely analyzed by either matrix-assisted laser desorption/ionization time-of-flight (MALDI-TOF) or electrospray ionization (ESI) mass spectrometry (MS). The probability of unwanted sulfate loss increases with the number of sulfate residues. Therefore, oversulfated GAG (with more than one sulfate residue per carbohydrate unit) are much more refractive to MS analysis. In this case, even using ESI as one of the softer ionization methods, this effect is a serious problem for the characterization of unknown samples because sulfate loss cannot be neglected even with optimized measurement conditions.[26] To our best knowledge, all sulfated oligosaccharides tend to undergo the loss of sulfate residues in the gas phase at MS conditions, and this problem is, of course, the more pronounced the higher the number of sulfate residues[27] is.

In 2013, Zaia stated vibrational excitation as one reason leading to the rearrangement of protonated sulfate residues, which results in a loss of the functional group on the subsequently detected ion.[28] This effect is pronounced to a lesser extent for (a) deprotonated sulfate residues or (b) residues capable of ion pairing to a stabilizing cation. For highly sulfated GAG oligosaccharides, this leads to highly charged ion species in the negative ion mode because the charge state *z* is equal to the number of sulfate residues—a strongly sulfated oligosaccharide with more than four sulfate residues requires high-resolution MS measurements because, otherwise, these ions cannot be adequately characterized. This is a particular problem if low-resolution mass spectrometers have to be used. Such mass spectrometers are, however, exclusively available in many laboratories, and thus, investigations on how optimum spectra can be obtained are important.

Furthermore, the desalination of analytes with such high charge density has to be carefully performed to provide a sufficient number of stabilizing cations for the formation of positive ion species without

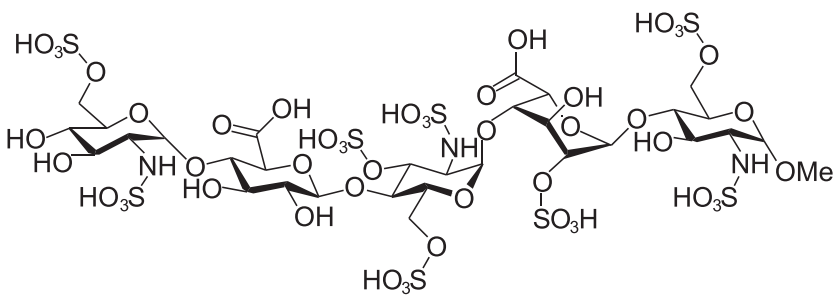

FIGURE 1 Chemical structure of fondaparinux. D-GlcNS6S-α-(1,4)-D-GlcA-β-(1,4)-D-GlcNS3,6S-α-(1,4)-L-IdoA2S-α-(1,4)-D-GlcNS6S-OMe; M_{Fpx} = 1506.95 (monoisotopic)

interfering with the quality of ESI mass spectra, for example. We tested different desalination methods and optimized the measurement conditions using a commercially available (in physiological salt solution) model compound: fondaparinux is a synthetic pentasaccharide with eight sulfate residues shown in Figure 1. It is structurally similar to the heparin-binding motif for the anticoagulant factor antithrombin III and widely used as an effective anticoagulant.[29] From a mass spectrometrist's viewpoint, however, this molecule is ideally suited as a model compound to study the sulfate loss in the gas phase. Therefore, it has been already used as a model compound for testing the performances of ionic liquid MALDI matrices[30] as well as ESI MS.[31]

Using this compound, we investigated the impact of different desalination protocols on the shape and the quality of the ESI mass spectra and the achievable sensitivity. In addition to sodium chloride, we also used quaternary ammonium salts as alternative counterions as described by Gunay et al.[32] After optimization of the measurement conditions for the positive and negative ion mode, we could establish a gentle and fast method for the ESI MS characterization of artificially sulfated GAG oligosaccharides by which particularly unwanted sulfate loss could be minimized.

Further MS^n investigations were not in the scope of this work because the majority of our compounds of interest are persulfated molecules, and with that, no positional isomers have to be distinguished. However, traditional CID (collision-induced) is normally not the method of choice because the obtained fragment ion spectra are normally dominated by peaks corresponding to the sulfate loss. Therefore, more sophisticated methods are regularly used.[33–35]

Chemoenzymatic approaches were used to synthesize completely sulfated or GAG oligosaccharides with defined sulfation patterns as well as different end group functionalizations.[36–38] This allows the investigation of the influence of the number of sulfate residues and the chain length on the binding affinity of GAG-derived oligosaccharides to specific mediator proteins utilizing different methods such as nuclear magnetic resonance (NMR) or hydrogen–deuterium exchange (HDX) MS.[39–43] A detailed characterization of these GAG analogues is mandatory to enable the correct interpretation of the biological effects of GAG upon their interactions with cells and proteins.

In a nutshell, our protocol enabled us to obtain reliable mass spectra in both (negative and positive) ion modes and even for highly negatively charged GAG derivatives with up to 16 sulfate residues. According to our best knowledge, compounds with such a huge number of sulfate residues were not yet investigated by MS.

2 | MATERIALS AND METHODS

2.1 | Materials

All chemicals for sample preparation and all solvents were obtained in the highest commercially available purity from Sigma-Aldrich (now owned by the Merck company) and used as supplied. Fondaparinux (D-GlcNS6S-α-(1,4)-D-GlcA-β-(1,4)-D-GlcNS3,6S-α-(1,4)-L-IdoA2S-α-(1,4)-D-GlcNS6S-OMe) was purchased from Glaxo Smith Kline as 12 mg ml^{-1} syringe solutions for direct injections with physiological salt concentration (154-mM NaCl). HA oligosaccharides **1–9** (shown in Figure 6) with defined sulfation patterns were obtained by chemoenzymatic conversion of hyaluronic acid as described in references.[36–38]

2.2 | Sample preparation

2.2.1 | Desalination via dialysis

Fondaparinux was desalted using Biotech cellulose ester tubing with a molecular weight cutoff of 100–500 Da prior to ESI MS analysis. Fondaparinux was dialyzed against deionized water for 5 days, similar to the protocol described in Jen and Leary.[31] In parallel, dialysis against tetraethylammonium hydroxide solution (TEA OH) 0.1% (V/V) was performed under identical conditions.

2.2.2 | Cation exchange

In order to replace all alkali ions by quaternary ammonia ions, a Dowex 50WX8 (Sigma-Aldrich) strongly acidic cation exchange column (1.2 × 10 cm, containing the resin) was used. The sodium salt of the analyte was dissolved in deionized water (Millipore) to a final concentration of 5 mg ml^{-1}. The cation exchange column was equilibrated with 4 ml of 2-M aqueous HCl and subsequently washed with deionized water. Afterwards, 2 ml of the analyte solution was slowly applied onto the column with a Pasteur pipette and then eluted with water. At least four different fractions of 3 ml were collected and the pH value was measured. The presence of carbohydrates was confirmed by a drop test: 0.5 µl of each fraction was spotted onto a standard (silica gel) thin layer chromatography (TLC) plate, which was afterwards stained with orcinol/H_2SO_4.[44] The fractions of interest were neutralized with TEA OH and one sample was kept as the protonated form.

2.2.3 | Desalination via size exclusion column

The column (PD MiniTrap G-10-2.1 ml Sephadex G-10) was equilibrated with 8 ml deionized water (Millipore). Afterwards, a maximum of 0.35 ml of the analyte solution was applied onto the column and subsequently eluted with water (Millipore). Fractions of 0.5 ml were collected and the presence of the analyte was confirmed as described above.

2.2.4 | Concentration determination

The concentration of the analyte after desalination was performed by using the modified uronic acid carbazole reaction.[45] For calibration,

different samples with known concentrations of fondaparinux were used.

2.3 | ESI MS measurements

Carbohydrate analysis was carried out by ESI MS by using an Amazon SL ion trap (IT) mass spectrometer (Bruker Daltonics, Bremen, Germany). Nitrogen was used as the nebulizer gas at 7.25 psi. The samples in methanol–water 1/1 (V/V) were introduced into the ESI source via a syringe pump at two slightly different conditions: B1 (sample flow 3 μl min^{-1}, dry gas temperature 180°C, dry gas flow 4 L min^{-1}) and B2 (sample flow 5 μl min^{-1}, dry gas temperature 200°C, dry gas flow 8 L min^{-1}). Data acquisition and analysis were performed using the programs TrapControl and DataAnalysis, respectively (Bruker Daltonics, Bremen, Germany). All spectra were acquired with a mass accuracy of about 10 ppm, that is, all *m/z* values show deviations of ±0.01 *m/z*.

3 | RESULTS AND DISCUSSION

3.1 | Comparison of desalination protocols: Duration and recovery rates

Because non-volatile salts such as NaCl and other alkali halogenides have a strong (negative) impact on ESI and the quality of mass spectra, desalination is a crucial step in the sample preparation for direct infusion ESI MS. We employed three different approaches: desalination via dialysis, cation exchange, and desalination via a size exclusion column (SEC). The molecular weight cut-off of the dialysis tube restricts the minimal size of the analytes. Unfortunately, there is a considerable loss of the (relatively small) oligosaccharides and the recovery rate after dialysis is just about 20%. Sufficient desalination was achieved after 5 days of dialysis against water as well as against a solution of tetraethylammonium salts. In contrast, cation exchange is suitable for a wide range of molecular weights, requires less time (about 2 h), and yields the analytes exclusively in the protonated form. Nevertheless, this confers a low pH value (lower than 2) that might induce unwanted hydrolysis (degradation) of the carbohydrates. Neutralization with salt solutions such as tetraethyl ammonium hydroxide prevents unwanted degradation reactions. The recovery rate was about 35%. Gel filtration or size exclusion chromatography (SEC) was the fastest among the tested methods (around 30 min) and feasible for disaccharides already. The recovery rate was around 40%. The desalination via SEC, however, was incomplete. The desalination capacity should be above 94% according to the information provided by the manufacturer of the columns. We tested this with measurement of the electrical conductivity of SEC-desalinated fondaparinux samples (data not shown), and we resulted in an extent of desalination of about 90%. These samples were diluted with methanol 1:1 (V:V) down to 1.0 mg ml^{-1} carbohydrate, which is equal to an NaCl concentration of about 0.1 mg ml^{-1}, and were used for the optimization of the measurement conditions.

3.2 | ESI IT MS: Optimization

The measurement conditions were optimized separately for the two (positive and negative) acquisition modes. The mass to charge (*m/z*) range was as wide as possible (80–2,200 *m/z*) to make the optimized conditions feasible for a wider mass range of analytes at a later stage. The voltage on the capillary was varied between 500 and 5,000 V during these measurements to find optimal conditions, that is, the maximum of analyte intensity and minimum yields of fragmentation products. Multiply charged intact analyte ion species are detected in both polarity modes due to the polyelectrolyte character of the analyte of interest and exhibit different numbers of counterions. The detailed assignments of the *m/z* ratios are given in Table S1 and only some selected peaks are assigned directly at the corresponding spectra.

The dependency of the mass spectra on the measurement conditions is illustrated in Figure 2. The mass spectra in the negative ion mode (Figure 2, Traces 1 to 4) look very similar at the first glance: the most intense signals between *m/z* 300 and 700 correspond to multiply charged intact analyte ions, less intense smaller carbohydrate fragment ions, and multiply charged analyte clusters. Comparing Traces 1 and 3 (respectively 2 and 4) shows that the extent of analyte clustering increases (expectedly) with the higher sample amount per time but is also affected to an even higher extent by the trap drive level, which will be explained below in more detail.

These differences are even more pronounced in the positive ion mode: the mass spectra provide evidence of abundant sodium chloride clusters beside multiply charged analyte ions for a trap drive level of 50% (Trace 5), which complicated the assignment of the signals. These sodium chloride clusters are not detectable for 100% trap drive level under otherwise identical conditions (Trace 6). In contrast, the formation of multiply charged analyte clusters for higher sample flow rates is not affected by the higher trap drive level (Trace 8). Table 1 shows the corresponding parameters as well as the percentages of the assigned ion species, the extent of sulfate loss, cleavage of glyosidic linkages, sodium chloride, and analyte clusters and intact analyte ion species. Furthermore, the assignment and the signal intensity of the most abundant intact analyte ion species is given, which confirms clear differences in sensitivity.

The trap drive level as one parameter of the smart parameter setting (SPS) of the used ESI IT mass spectrometer measures the amplitude of the main high radio frequency voltage on the ring electrode of the IT, which generates the pseudopotential at which the ions are moving. The trap drive level depends on the used frequency and other measurement and device-specific parameters. In general, trapping ions with higher *m/z* ratios requires higher trap drive levels, which also depends on the kinetic energy of the ions and with that on the upstream ion optics. The parameter *compound stability* as a parameter of the ion optic for the gentle ion transfer into the IT was set to 50% in all the discussed experiments with highly sulfated oligosaccharides. The selected trap drive level has a more pronounced impact on the signal intensities than the electrospray conditions even though B2 brings more analyte molecules to ionization than B1. A trap drive level

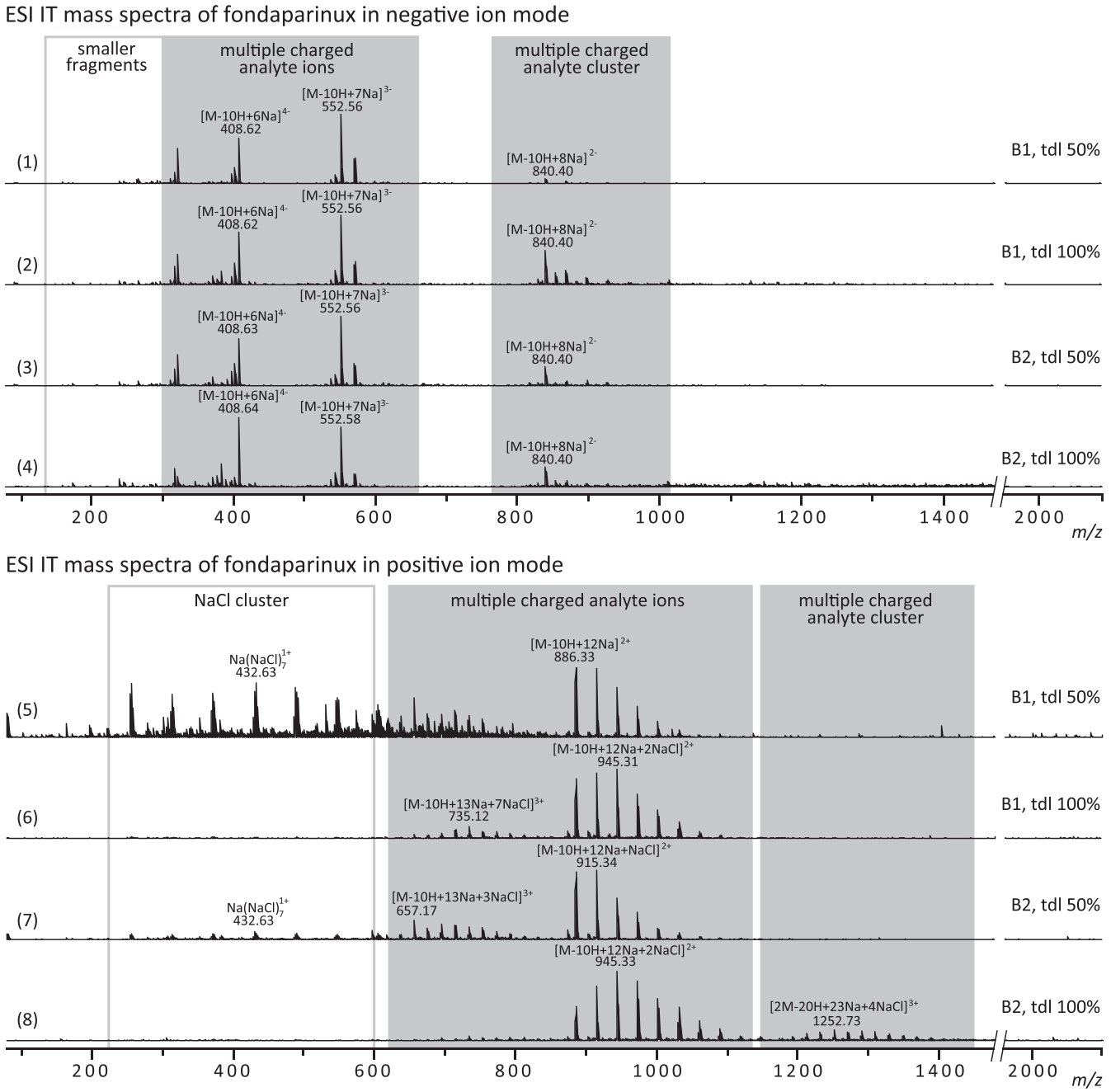

FIGURE 2 Electrospray ionization ion trap mass spectra of fondaparinux. Recorded in the positive and negative ion mode for two different (flow rate) electrospray conditions and trap drive levels, respectively. The utilized conditions were B1 (sample flow 3 µl min^{-1}, dry gas temperature 180°C, dry gas flow 4 L min^{-1}) and B2 (sample flow 5 µl min^{-1}, dry gas temperature 200°C, dry gas flow 8 L min^{-1}). The mass spectra in negative ion mode show series of multiply charged analyte ions (different charge states and different amount of sodium counterions) beside a series of multiply charged analyte clusters differing in the number of sodium atoms as well as small amounts of smaller fragment ions due to in-source decay of the glycosidic bonds. The mass spectra in positive ion mode exhibit series on sodium chloride clusters, multiply charged analyte ions, and analyte clusters. Detailed assignments of the observed *m/z* ratios can be found in Table S1, whereas only the most intense peaks are assigned at the respective mass spectra

of 100% results in higher signal intensities than 50%. Again, the negative ion mode is characterized by a typical behavior, which differs from positive ion detection: higher signal intensities are achieved with a trap drive level of 50%. A simple explanation is the suppression of analyte signals in the positive ion mode due to (residual) NaCl clustering. Relatively harsh trap conditions with 100% trap drive level discriminate these clusters during the trapping. This allows more analyte ions to accumulate in the trap and their subsequent detection, even as clusters at high sample concentrations. This also applies for negative polarity; however, the measurements provide evidence that the negative ions are more sensitive to fragmentation and undergo elevated loss of sulfate groups. Hence, a lower trap drive level of 50%

TABLE 1 Results of electrospray ionization mass spectrometry of selected fondaparinux samples

	Cond.	tdl	Assigned	% Intact	% Fragment ions	% SO_3 loss	% NaCl cluster	% M cluster	I_{max}/Mio. counts	*m/z*	*z*	Assignment
–	B1	50%	96%	90%	9%	2%	0%	0%	11,6	552.56	3	M + 7Na
–	B1	100%	98%	57%	12%	8%	1%	23%	7,2	552.56	3	M + 7Na
–	B2	50%	98%	76%	11%	5%	0%	8%	10,8	552.56	3	M + 7Na
–	B2	100%	89%	53%	17%	12%	0%	17%	5,8	408.64	4	M + 6Na
+	B1	50%	40%	66%	0%	0%	34%	0%	0,2	886.33	2	M + 12Na
+	B1	100%	99%	99%	0%	0%	1%	0%	5,8	915.33	2	M + 12Na + NaCl
+	B2	50%	95%	89%	0%	0%	8%	0%	1,6	915.34	2	M + 12Na + NaCl
+	B2	100%	94%	85%	0%	0%	0%	15%	6,8	945.33	2	M + 12Na + 2NaCl

Note. The utilized conditions were B1 (sample flow 3 μl min^{-1}, dry gas temperature 180°C, dry gas flow 4 L min^{-1}) and B2 (sample flow 5 μl min^{-1}, dry gas temperature 200°C, dry gas flow 8 L min^{-1}) in both polarities (+, –). Furthermore, two different values for the trap drive level (tdl) were used (50% and 100%). The moieties of intact analyte ions, fragment ions, sulfate loss, and clusters on the overall assigned signals are given. In addition to the intensities of the base peaks, the *m/z* value, the charge state, and the assignment are also given. All values are given with an estimated mass accuracy of ±0.01 *m/z*.

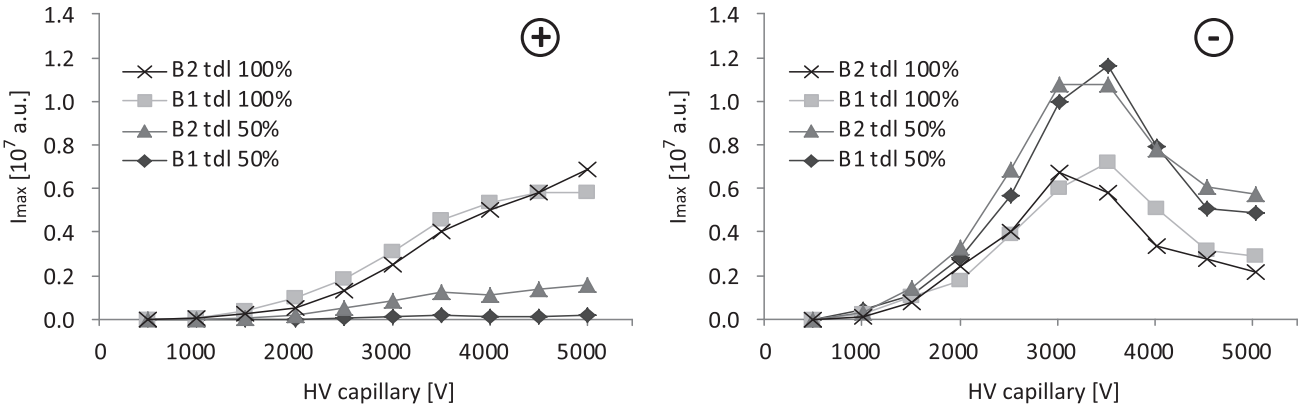

FIGURE 3 Intensity of the most intense signal in the electrospray ionization mass spectra of fondaparinux in dependence on the high voltage applied to the capillary. In the positive ion mode, a clear dependency of the signals on the capillary voltage with increasing intensities for higher voltages is obvious (left). The signal intensities in the negative ion mode show a maximum at about 3,500 V (right). Overall, the negative ion mode provides higher signal intensities and is thus more sensitive towards fondaparinux and similar analytes. (tdl, trap drive level; B1: sample flow 3 μl min^{-1}, dry gas flow 4 L min^{-1}, dry gas temperature 180°C; B2: sample flow 5 μl min^{-1}, dry gas flow 8 L min^{-1}, dry gas temperature 200°C)

leads to reduced fragmentations and, consequently, more intact analyte ions.

Figure 3 shows the impact of the capillary high voltage on the intensity of the intact analyte ion species. Here, the signal intensities in the positive ion mode correlate directly with the high voltage applied to the capillary, whereas the intensities in the negative ion mode exhibit a maximum at about 3,500 V and higher voltages lead to a reduction of the peak intensities.

3.3 | Comparison of desalination protocols: ESI IT mass spectra

The fondaparinux samples after different desalination protocols give very different mass spectra under the optimized measurement conditions as illustrated in Figure 4. It is evident that the number and the type of the counterions determine the stability and the formation of adducts of the analyte during the ionization process and, of course, lead to different *m/z* ratios, which can be easily differentiated even at poor resolution and poor mass accuracy. Fondaparinux can be detected at our experimental conditions in the negative ion mode regardless of the used desalination method. Of course, the counterions and thus the observed adducts are different: residual NaCl leads to intense sodium adducts after dialysis against water (1) and size exclusion chromatography (5) and the most intense signals correspond to multiply charged ions $[M\text{-}8H + 4Na]^{4-}$ at *m/z* 397.65 and $[M\text{-}6H + 3Na]^{3-}$ at *m/z* 537.90. Residual TEA leads to similar ion formation: $[M\text{-}10H + 5TEA]^{5-}$ at *m/z* 429.49, $[M\text{-}10H + 6TEA]^{4-}$ at *m/z* 569.69, and $[M\text{-}10H + 7TEA]^{3-}$ at *m/z* 803.00 as in (2) and (4).

Cleavage of the glycosidic linkages and loss of sulfate groups occur in the absence of a sufficient number of counterions, that is,0 $[M\text{-}3SO_3\text{-}3H]^{3-}$ at *m/z* 421.30, $[M\text{-}4SO_3\text{-}4H]^{3-}$ at *m/z* 394.64, $[Y_1\text{-}SO_3H]^{1-}$ at *m/z* 271.97, and $[Y_4\text{-}4SO_3 + 3Na\text{-}4H]^{2-}$ at *m/z* 464.99. This is particularly the case after cation exchange without neutralization (3), and intact analyte ion species are not detectable at

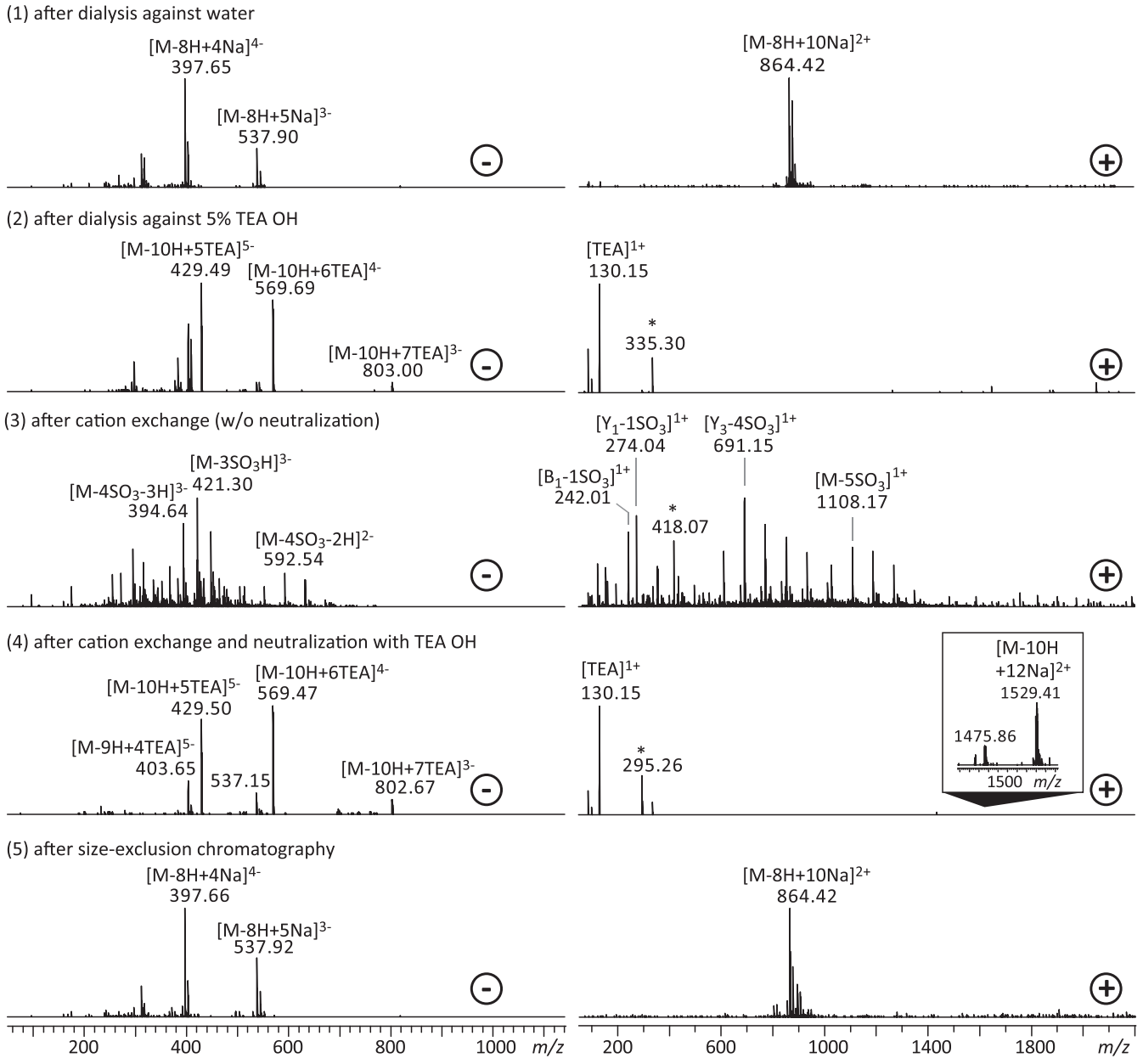

FIGURE 4 Electrospray ionization (ESI) mass spectra of selected fondaparinux samples after different desalination protocols. The ESI ion trap mass spectra of fondaparinux after five different desalination protocols were recorded in both polarities (+, –) under the corresponding optimized measurement conditions mentioned above. Sample preparations: dialysis against water (1), dialysis against a 5% TEA OH solution (2), cation exchange without neutralization (3), or using neutralization with TEA OH (4) afterwards as well as desalination via size exclusion (5). The sample concentration for the measurements was 1 mmol L^{-1}. Detailed assignments of the observed *m/z* values can be found in Table S2

these conditions. The neutralization with TEA OH (Trace 4) stabilizes the analyte during the ionization process, which excludes severe hydrolysis of the sulfoesters under the acidic conditions during the desalination process.

This effect is more pronounced in the positive ion mode: most intense signals can be assigned to fragment ions, that is, $[Y3\text{-}4SO_3]^{1+}$ at *m/z* 691.15, $[Y3\text{-}3SO_3]^{1+}$ at *m/z* 771.10, $[Y1\text{-}1SO_3]^{1-}$ at *m/z* 274.04, or species after losses of several sulfate residues such as $[M\text{-}5SO_3\text{-}1H]^{1-}$ at *m/z* 1108.17 after cation exchange without any neutralization (3). The in-source decay of the carbohydrate as a cleavage of the glycosidic bonds is very prominent under these conditions and is observable in both polarities. Fragment ions are labeled using the nomenclature of Domon and Costello.[46] A survey of the detected fragment ions is given in Figure S3.

Again, dialysis against water (1) and size exclusion chromatography (5) result in very similar, clean mass spectra with the base peak at *m/z* 864.42 assigned to $[M\text{-}12H + 10Na]^{2+}$. The positive ion mass spectra show very intense signals of the $[TEA]^{+}$ at *m/z* 130.15 in the case of volatile TEA as counterion, that is, after dialysis against TEA OH (2) and after cation exchange and neutralization with TEA OH (4). These signals discriminate the analyte signals at about *m/z* 1,500. Detailed assignments of the

peaks detected in the respective mass spectra are available in the supporting information.

3.4 | Comparison of desalination protocols: ESI IT MS sensitivity

The positive and negative ion mass spectra of fondaparinux after the different desalination protocols were recorded for seven different analyte concentrations ranging from 1 μmol L^{-1} to 1 mmol L^{-1} to estimate the sensitivity of ESI MS towards highly sulfated oligosaccharides. A comparison of these intensities is shown in Figure 5, except the cation exchange samples without neutralization, because no intact analyte ion species are detected at these conditions at all, independent of the polarity. The mass range is *m/z* 80 to 2,200 for both the positive and the negative ion mode. Because TEA ions give a very intense but unwanted signal at *m/z* 130 in the positive ion mode, a second set of mass spectra was recorded with a limited range of *m/z* 400 to 2,200. In all cases, the negative ion mode yields higher intensities compared with the corresponding measurements in the positive ion mode.

Intact fondaparinux ions are detectable down to 1 μmol L^{-1} in both detection modes after desalination by dialysis against water. Size exclusion chromatography yields similar results, though it is less sensitive with the analyte not being detectable in the positive ion mode at the lowest tested concentration. The picture changes for TEA as the counterions: intact analyte ions are detectable in the negative ion mode after dialysis against TEA solution and after cation exchange to TEA, but with a much lower sensitivity compared with the other two desalination methods. There are no positively charged, intact analyte ions detectable at all for the extended measuring range and only low yields for the higher sample concentrations in the case of the limited measuring range. This is due to the intense TEA^+ signals at *m/z* 130 and other TEA clusters suppressing the analyte ions of interest.

The intensity of the intact analyte ion species peak is higher for lower concentrations in the case of negative ion detection after cation exchange with TEA, indicating a dilution effect: with slightly smaller amounts of analyte, improved effects can be obtained because the suppressing TEA signals are less intense. Even after dialysis, the dilution effect is observable and points out that an optimal ratio between counterions and analyte molecules is hard to obtain with TEA as the counterions. Therefore, we discarded this approach for further investigations and used size exclusion desalination for faster and reliable measurements.

3.5 | Characterization of defined or fully sulfated GAG oligosaccharides with different anomeric functionalizations

In the case of carbohydrates with a defined sulfation pattern or completely sulfated oligosaccharides with different anomeric ligations, fast and reliable MS characterization is desirable, because a reliable statement regarding the number of sulfate residues and the attached anomeric functional groups can be made directly from the measured

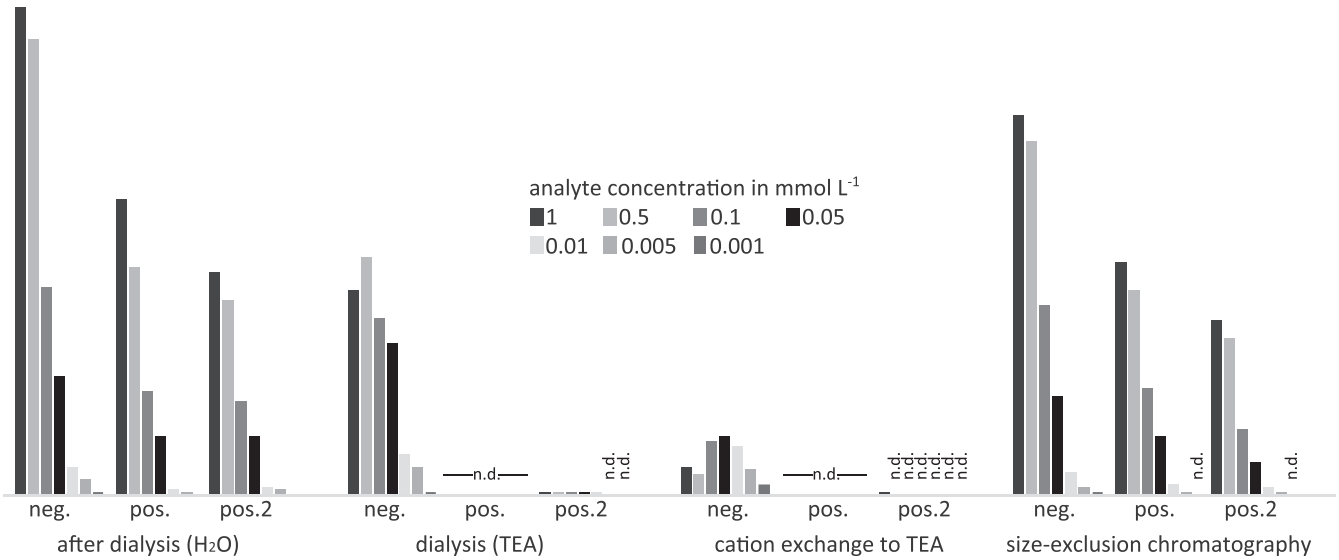

FIGURE 5 Intensities of the most intense intact ion peaks of fondaparinux in the electrospray ionization mass spectra. Four different desalination protocols were evaluated: dialysis against water (dia H_2O), dialysis against TEA OH solution (dis TEA), cation exchange to TEA counterions (cation exchange TEA), and size exclusion chromatography. In each case, the intensities of the most abundant intact analyte ion species were monitored for the positive and the negative ion mode in a large measuring range between 80 and 2,200 *m/z* (pos and neg) as well as for positive ion mode in a restricted measuring range, that is, between 400 and 2,200 *m/z* (pos 2). The cation exchange without neutralization is not shown because only fragment ions were detected independent of the polarity. The sample concentration was varied between 1 μmol L^{-1} and 1 mmol L^{-1} (n.d. = not detected)

m/z ratio. Based on this work, artificially sulfated HA oligosaccharides with different anomeric ligations were characterized using ESI MS. These were defined sulfated species with different degrees of polymerization from disaccharides to hexasaccharides. In addition to azides and thiols, tetramethyl rhodamine labels were also introduced by anomeric ligation; these structures are shown in Figure 6. Furthermore, two maleimides and three acrylates were characterized during this work (structures not shown). Mass spectra and the corresponding assignments can be found in the supporting information.

The different end groups, which cause different physicochemical properties and thus change the MS properties, were challenging. For example, in the case of the azide complexes, a mass loss of $\Delta m/z = 43.02$ was found. This corresponds to a loss of HN_3 caused by in-source fragmentation during the ESI process as described in the literature before.[47]

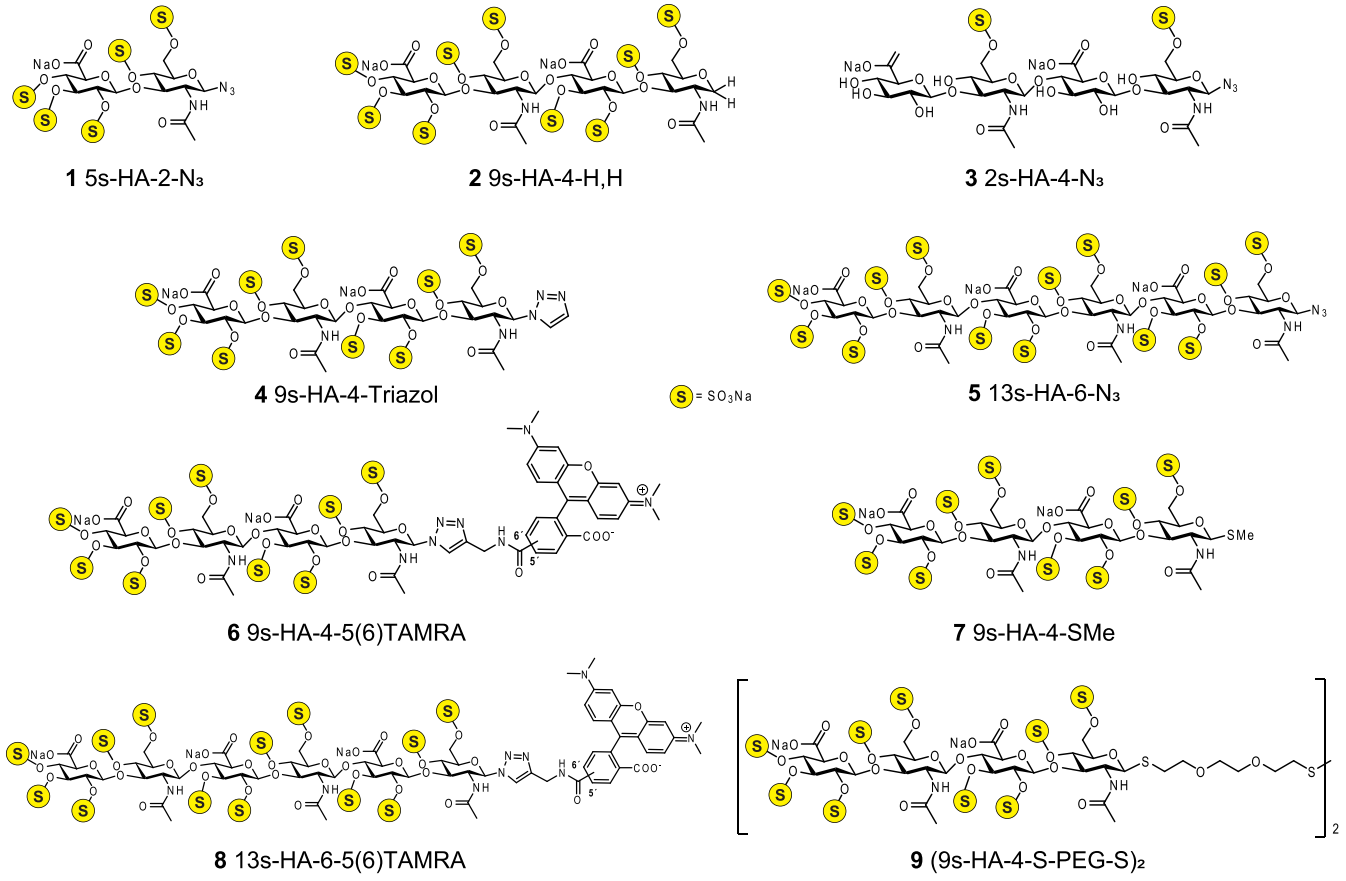

FIGURE 6 Chemical structures of defined sulfated oligohyaluronans with different functionalizations of the anomeric end. These compounds differ not only in their molecular weight between ~800 and 3,500 Da but also in the number of sulfate residues. **1** 5s-HA-2-N_3: 2,3,4-tri-*O*-sulfo-β-D-glucopyranuronyl-(1→3)-4,6-di-*O*-sulfo-β-D-2-acetamido-2-deoxy-glucopyranosyl-1-azide; 2 9s-HA-4-N_3: 2,3,4-tri-*O*-sulfo-β-D-glucopyranuronyl-(1→3)-4,6-di-*O*-sulfo-β-D-2-acetamido-2-deoxy-glucopyranosyl-(1→4)-2,3-di-*O*-sulfo-β-D-glucopyranuronyl-(1→3)-4,6-di-*O*-sulfo-β-D-2-acetamido-1,5-anhydro-2-deoxy-sorbitol; 3 2s-HA-4-N_3: β-D-glucopyranuronyl-(1→3)- β-D-2-acetamido-2-deoxy-6-sodium sulfo-glucopyranosyl-(1→4)- β-D-glucopyranuronyl-(1→3)- β-D-2-acetamido-2-deoxy-6-sodium sulfo-glucopyranosyl-1-azide; 4 9s-HA-4-triazol: 2,3,4-tri-*O*-sulfo-β-D-glucopyranuronyl-(1→3)-4,6-di-*O*-sulfo-β-D-2-acetamido-2-deoxy-glucopyranosyl-(1→4)-2,3-di-*O*-sulfo-β-D-glucopyranuronyl-(1→3)-4,6-di-*O*-sulfo-β-D-2-acetamido-2-deoxy-glucopyranosyl-1,2,3-triazol; 5 13s-HA-6-N_3: 2,3,4-tri-*O*-sulfo-β-D-glucopyranuronyl-(1→3)-4,6-di-*O*-sulfo-β-D-2-acetamido-2-deoxy-glucopyranosyl-(1→4)-2,3,4-tri-*O*-sulfo-β-D-glucopyranuronyl-(1→3)-4,6-di-*O*-sulfo-β-D-2-acetamido-2-deoxy-glucopyranosyl-(1→4)-2,3-di-*O*-sulfo-β-D-glucopyranuronyl-(1→3)-4,6-di-*O*-sulfo-β-D-2-acetamido-2-deoxy-glucopyranosyl-1-azide; 6 9s-HA-4-TAMRA: 2,3,4-tri-*O*-sulfo-β-D-glucopyranuronyl-(1→3)-4,6-di-*O*-sulfo-β-D-2-acetamido-2-deoxy-glucopyranosyl-(1→4)-2,3-di-*O*-sulfo-β-D-glucopyranuronyl-(1→3)-4,6-di-*O*-sulfo-β-D-2-acetamido-2-deoxy-glucopyranosyl-1,2,3-triazol-4-yl-methyl-2-carbamoyl-5(6)-carboxytetramethylrhodamine; 7 9s-HA-4-SMe: 2,3,4-tri-*O*-sulfo-β-D-glucopyranuronyl-(1→3)-4,6-di-*O*-sulfo-β-D-2-acetamido-2-deoxy-glucopyranosyl-(1→4)-2,3-di-*O*-sulfo-β-D-glucopyranuronyl-(1→3)-4,6-di-*O*-sulfo-β-D-2-acetamido-2-deoxy-glucopyranosyl-1-thio-methyl; 8 13s-HA-6-TAMRA: 2,3,4-tri-*O*-sulfo-β-D-glucopyranuronyl-(1→3)-4,6-di-*O*-sulfo-β-D-2-acetamido-2-deoxy-glucopyranosyl-(1→4)-2,3,4-tri-*O*-sulfo-β-D-glucopyranuronyl-(1→3)-4,6-di-*O*-sulfo-β-D-2-acetamido-2-deoxy-glucopyranosyl-(1→4)-2,3-di-*O*-sulfo-β-D-glucopyranuronyl-(1→3)-4,6-di-*O*-sulfo-β-D-2-acetamido-2-deoxy-glucopyranosyl-1,2,3-triazol-4-yl-methyl-2-carbamoyl-5(6)-carboxytetramethylrhodamine; 9 2,3,4-tri-*O*-sulfo-β-D-glucopyranuronyl-(1→3)-4,6-di-*O*-sulfo-β-D-2-acetamido-2-deoxy-glucopyranosyl-(1→4)-2,3-di-*O*-sulfo-β-D-glucopyranuronyl-(1→3)-4,6-di-*O*-sulfo-β-D-2-acetamido-2-deoxy-glucopyranosyl-1-thio-2-ethyloxy-2-ethylox-2-ethyl-disulfide. The corresponding mass spectra in the positive ion mode for all compounds of interest and in negative ion mode for selected compounds as well as the assignments of the detected peaks are given in Table S4

Because the sulfate group loss in the positive ion mode is almost negligible under these optimized ESI conditions, it would be desirable for the determination of the position of the sulfate groups in the case of defined sulfated derivatives if fragmentation by means of MS^2 would provide the desired positional information. However, fragmentation of the corresponding positive ions did not lead to a satisfactory result: all the spectra were dominated by peaks corresponding to sulfate loss, whereas all other peaks were characterized by poor intensities.

4 | CONCLUSION

In the present work, we established an improved protocol for the characterization of oligosaccharides with defined sulfation patterns via ESI MS, which is suitable for different numbers of sulfate groups, molecular weights, and end group modifications and yields a minimized extent of side reactions such as sulfate loss or other in-source decay reactions.

The already established methods for desalination and ESI MS measurements are often optimized for a particular molecular weight, which limits their applications for a broader range of similar analytes: in our case, the molecular weight cut-off of the dialysis material excludes smaller analytes such as disaccharides due to the very low recovery rates. Cation exchange is much more difficult for analytes with, for instance, acidic functional groups. Using small size exclusion columns is relatively fast and suitable for a broad range of molecular weights. Finally, the remaining sodium chloride (as the consequence of incomplete desalination) provides a sufficient number of counterions to stabilize the sulfate residues and the glycosidic bonds during the ionization process. Therefore, SEC is the method of choice for the discussed oligosaccharides—at least among the discussed desalination methods.

Our findings illustrate that highly sulfated oligosaccharides behave very differently depending on the polarity: the negative ion mode is much more sensitive at the optimal capillary voltage than the positive ion mode. However, the negatively charged ions are more sensitive towards glycosidic bond cleavage and sulfate loss. In contrast, positively charged ions are more stable. To generate these positive ions, a sufficient amount of counterions is indispensable, which could lead to sodium chloride clusters and TEA contaminations and therefore has to be carefully adjusted.

ACKNOWLEDGEMENTS

This work was supported by the German Research Council (DFG)—project 59307082—TRR67/A8 & Z3. We would also like to thank all our colleagues who helped us in performing the related experiments.

Open Access funding enabled and organized by ProjektDEAL. WOA Institution: UNIVERSITAET LEIPZIG Blended DEAL: ProjektDEAL

CONFLICT OF INTEREST

The authors declare no conflict of interest.

ORCID

Katharina Lemmnitzer https://orcid.org/0000-0001-9328-7319

REFERENCES

1. Theocharis AD, Skandalis SS, Gialeli C, Karamanos NK. Extracellular matrix structure. *Adv Drug Deliv Rev*. 2016;97:4-27.
2. Schnabelrauch M, Scharnweber D, Schiller J. Sulfated glycosaminoglycans as promising artificial extracellular matrix components to improve the regeneration of tissues. *Curr Med Chem*. 2013;20(20):2501-2523.
3. Reitinger S, Lepperdinger G. Hyaluronan, a ready choice to fuel regeneration: a mini-review. *Gerontology*. 2013;59(1):71-76.
4. DeAngelis PL. Glycosaminoglycan polysaccharide biosynthesis and production: today and tomorrow. *Appl Microbiol Biotechnol*. 2012;94(2):295-305.
5. Sasisekharan R, Venkataraman G. Heparin and heparan sulfate: biosynthesis, structure and function. *Curr Opin Chem Biol*. 2000;4(6):626-631.
6. Evanko SP, Angello JC, Wight TN. Formation of hyaluronan- and versican-rich pericellular matrix is required for proliferation and migration of vascular smooth muscle cells. *Arterioscler Thromb Vasc Biol*. 1999;19(4):1004-1013.
7. Rozario T, DeSimone DW. The extracellular matrix in development and morphogenesis: a dynamic view. *Dev Biol*. 2010;341(1):126-140.
8. Wight TN. Provisional matrix: a role for versican and hyaluronan. *Matrix Biol*. 2017;60–61:38-56.
9. Maldonado M, Nam J. The role of changes in extracellular matrix of cartilage in the presence of inflammation on the pathology of osteoarthritis. *Biomed Res Int*. 2013;2013:1-10.
10. Multhaupt HAB, Leitinger B, Gullberg D, Couchman JR. Extracellular matrix component signaling in cancer. *Adv Drug Deliv Rev*. 2016;97:28-40.
11. Benders KEM, van Weeren PR, Badylak SF, Saris DBF, Dhert WJA, Malda J. Extracellular matrix scaffolds for cartilage and bone regeneration. *Trends Biotechnol*. 2013;31(3):169-176.
12. Volpi N. Therapeutic applications of glycosaminoglycans. *Curr Med Chem*. 2006;13(15):1799-1810.
13. Järveläinen H, Sainio A, Koulu M, Wight TN, Penttinen R. Extracellular matrix molecules: potential targets in pharmacotherapy. *Pharmacol Rev*. 2009;61(2):198-223.
14. Liang J, Jiang D, Noble PW. Hyaluronan as a therapeutic target in human diseases. *Adv Drug Deliv Rev*. 2016;97:186-203.
15. Köwitsch A, Zhou G, Groth T. Medical application of glycosaminoglycans—a review. *J Tissue Eng Regen Med*. 2018;12(1):e23–e41.
16. Ateshian GA, Rajan V, Chahine NO, Canal CE, Hung CT. Modeling the matrix of articular cartilage using a continuous fiber angular distribution predicts many observed phenomena. *J Biomech Eng*. 2009;131(6):61003–61013.
17. Mattson JM, Turcotte R, Zhang Y. Glycosaminoglycans contribute to extracellular matrix fiber recruitment and arterial wall mechanics. *Biomech Model Mechanobiol*. 2017;16(1):213-225.
18. Gama CI, Hsieh-Wilson LC. Chemical approaches to deciphering the glycosaminoglycan code. *Curr Opin Chem Biol*. 2005;9(6):609-619.
19. Soares da Costa D, Reis RL, Pashkuleva I. Sulfation of glycosaminoglycans and its implications in human health and disorders. *Annu Rev Biomed Eng*. 2017;19(1):1-26.
20. Henrotin Y, Lambert C. Chondroitin and glucosamine in the management of osteoarthritis: an update. *Curr Rheumatol Rep*. 2013;15(10):361–370.
21. Fareed J, Iqbal O, Cunanan J, et al. Changing trends in anti-coagulant therapies. Are heparins and oral anti-coagulants challenged? *Int Angiol*. 2008;27(3):176–192.
22. Liu H, Zhang Z, Linhardt RJ. Lessons learned from the contamination of heparin. *Nat Prod Rep*. 2009;26(3):313-321.
23. Fu L, Li G, Yang B, et al. Structural characterization of pharmaceutical heparins prepared from different animal tissues. *J Pharm Sci*. 2013;102(5):1447-1457.

24. Pan J, Qian Y, Zhou X, Lu H, Ramacciotti E, Zhang L. Chemically oversulfated glycosaminoglycans are potent modulators of contact system activation and different cell signaling pathways. *J Biol Chem*. 2010;285(30):22966–22975.
25. Korn P, Schulz MC, Hintze V, et al. Chondroitin sulfate and sulfated hyaluronan-containing collagen coatings of titanium implants influence peri-implant bone formation in a minipig model. *J Biomed Mater Res A*. 2014;102(7):2334-2344.
26. Hu P, Fang L, Chess EK. Source-induced fragmentation of heparin, heparan, and galactosaminoglycans and application. *Anal Chem*. 2009;81(6):2332-2343.
27. Schiller J, Huster D. New methods to study the composition and structure of the extracellular matrix in natural and bioengineered tissues. *Biomatter*. 2012;2(3):115-131.
28. Zaia J. Glycosaminoglycan glycomics using mass spectrometry. *Mol Cell Proteomics*. 2013;12(4):885-892.
29. Kuo KHM, Kovacs MJ. Fondaparinux: a potential new therapy for HIT. *Hematology*. 2005;10(4):271-275.
30. Laremore TN, Zhang F, Linhardt RJ. Ionic liquid matrix for direct UV-MALDI-TOF-MS analysis of dermatan sulfate and chondroitin sulfate oligosaccharides. *Anal Chem*. 2007;79(4):1604-1610.
31. Jen CH, Leary JA. A competitive binding study of chemokine, sulfated receptor, and glycosaminoglycan interactions by nano-electrospray ionization mass spectrometry. *Anal Biochem*. 2010;407(1):134-140.
32. Gunay NS, Tadano-Aritomi K, Toida T, Ishizuka I, Linhardt RJ. Evaluation of counterions for electrospray ionization mass spectral analysis of a highly sulfated carbohydrate, sucrose octasulfate. *Anal Chem*. 2003;75(13):3226-3231.
33. Hawkridge AM, Hackbusch S. Ultraviolet photodissociation of fondaparinux generates signature antithrombin-like 3-O-sulfated -GlcNS3S6S- monosaccharide fragment (Y3/C3). *Anal Bioanal Chem*. 2020;412(28):7925-7935. https://doi.org/10.1007/s00216-020-02925-w
34. Wei J, Wu J, Tang Y, et al. Characterization and quantification of highly sulfated glycosaminoglycan isomers by gated-trapped ion mobility spectrometry negative electron transfer dissociation MS/MS. *Anal Chem*. 2019;91(4):2994-3001. https://doi.org/10.1021/acs.analchem.8b05283
35. Klein DR, Leach FE, Amster IJ, Brodbelt JS. Structural characterization of glycosaminoglycan carbohydrates using ultraviolet photodissociation. *Anal Chem*. 2019;91(9):6019-6026. https://doi.org/10.1021/acs.analchem.9b00521
36. Köhling S, Exner MP, Nojoumi S, Schiller J, Budisa N, Rademann J. One-pot synthesis of unprotected anomeric glycosyl thiols in water for glycan ligation reactions with highly functionalized sugars. *Angew Chem Int Ed*. 2016;55(50):15510-15514.
37. Köhling S, Kunze G, Lemmnitzer K, et al. Chemoenzymatic synthesis of nonasulfated tetrahyaluronan with a paramagnetic tag for studying its complex with interleukin-10. *Chem A Eur J*. 2016;22(16):5563-5574.
38. Köhling S, Blaszkiewicz J, Ruiz-Gómez G, et al. Syntheses of defined sulfated oligohyaluronans reveal structural effects, diversity and thermodynamics of GAG–protein binding. *Chem Sci*. 2019;10(3):866-878.
39. Künze G, Köhling S, Vogel A, Rademann J, Huster D. Identification of the glycosaminoglycan binding site of interleukin-10 by NMR spectroscopy. *J Biol Chem*. 2016;291(6):3100-3113.
40. Panitz N, Theisgen S, Samsonov SA, et al. The structural investigation of glycosaminoglycan binding to CXCL12 displays distinct interaction sites. *Glycobiology*. 2016;26(11):1209-1221.
41. Rother S, Samsonov SA, Hofmann T, et al. Structural and functional insights into the interaction of sulfated glycosaminoglycans with tissue inhibitor of metalloproteinase-3—a possible regulatory role on extracellular matrix homeostasis. *Acta Biomater*. 2016;45:143-154.
42. Koehler L, Samsonov S, Rother S, et al. Sulfated hyaluronan derivatives modulate TGF-β1: receptor complex formation: possible consequences for TGF-β1 signaling. *Sci Rep*. 2017;7(1210):1–11.
43. Pichert A, Samsonov SA, Theisgen S, et al. Characterization of the interaction of interleukin-8 with hyaluronan, chondroitin sulfate, dermatan sulfate and their sulfated derivatives by spectroscopy and molecular modeling. *Glycobiology*. 2011;22(1):134-145.
44. Brückner J. Estimation of monosaccharides by the orcinol–sulphuric acid reaction. *Biochem J*. 1955;60(2):200-205.
45. Bitter T, Muir HM. A modified carbazole method for uronic acid determination. *Anal Biochem*. 1962;4(4):330-334.
46. Domon B, Costello CE. A systematic nomenclature for carbohydrate fragmentations in FAB-MS/MS spectra of glycoconjugates. *Glycoconjugate J*. 1988;5(4):397-409. https://doi.org/10.1007/BF01049915
47. Xiao Q, Ju Y, Yang X, Zhao Y-F. Electrospray ionization mass spectrometry of AZT H-phosphonates conjugated with steroids. *Rapid Commun Mass Spectrom*. 2003;17(13):1405-1410.

SUPPORTING INFORMATION

Additional supporting information may be found online in the Supporting Information section at the end of this article.

How to cite this article: Lemmnitzer K, Köhling S, Freyse J, Rademann J, Schiller J. Characterization of defined sulfated heparin-like oligosaccharides by electrospray ionization ion trap mass spectrometry. *J Mass Spectrom*. 2021;56:e4692. https://doi.org/10.1002/jms.4692